

Quantitative Study of Shrinkage and Warpage Behavior for Microcellular and Conventional Injection Molding

Adam Kramschuster, Ryan Cavitt, Donald Ermer, Zhongbao Chen, Lih-Sheng Turng

Polymer Engineering Center, Department of Mechanical Engineering, University of Wisconsin – Madison, Madison, Wisconsin 53706-1572

This research investigated the effects of processing conditions on the shrinkage and warpage (S&W) behavior of a box-shaped, polypropylene part using conventional and microcellular injection molding. Two sets of 2^{6-1} fractional factorial design of experiments (DOE) were employed to perform the experiments and proper statistical theory was used to analyze the data. After the injection molding process reached steady state, molded samples were collected and measured using an optical coordinate measuring machine (OCMM), which had been evaluated using a proper R&R (repeatability and reproducibility) measurement study. By analyzing the statistically significant main and two-factor interaction effects, the results show that the supercritical fluid (SCF) content (nitrogen in this case, in terms of SCF dosage time) and the injection speed affect the S&W of microcellular injection molded parts the most, whereas pack/hold pressure and pack/hold time have the most significant effect on the S&W of conventional injection molded parts. Also, this study quantitatively showed that, within the processing range studied, a reduction in the S&W could be achieved with the microcellular injection molding process. POLYM. ENG. SCI., 45:1408–1418, 2005. © 2005 Society of Plastics Engineers

INTRODUCTION

Injection molding with microcellular plastics (MCPs) is capable of producing parts with excellent dimensional stability while using less material, lower injection pressure, and achieving a shorter cycle time. This process (also known as the MuCell process) blends atmospheric gas (generally nitrogen or carbon dioxide) at a high-pressure, high-temperature supercritical state with the polymer melt in the screw barrel to create a single-phase polymer-gas solution. To facilitate fast and homogeneous mixing of the gas and polymer and to maintain a single-phase solution prior to

injection, the melt pressurization pressure (MPP) inside the screw barrel is typically kept between 80 and 200 bar. This pressure level is approximately one order of magnitude higher than the typical back pressure (generally between 3 and 30 bar) employed with the conventional injection molding process. During microcellular injection molding the sudden pressure drop in the material as it flows through the nozzle triggers the thermodynamic instability of the polymer-gas solution. As a result, the gas starts emerging from the polymer-gas solution forming numerous microscale cells. Figure 1 shows the schematic of injection molding with MCPs as well as the characteristic microstructures at the center and edge of the test part cross section. The size of the cells depends on the amount and type of dissolved gas, the time allowed for foaming prior to solidification, the strength of the polymer matrix, and the cell density. One can also adjust the process conditions or employ nano- or microscale fillers to obtain different cell densities [1–5]. For a specific set of process conditions or for a fixed expansion ratio, the cell size decreases with increasing cell density. As shown in Fig. 1, the typical cell diameter in injection molded microcellular parts is on the order of 10–100 microns (as opposed to 250 microns or more with the conventional structural foam molding process).

While realizing part weight reduction by replacing material with gas, the microcells also serve as crack arrestors by blunting crack tips, thereby greatly enhancing part toughness [6]. For example, when properly prepared microcellular polystyrene (PS) has five times the impact strength of its unfoamed counterpart [7, 8]. The fatigue life of microcellular polycarbonate (PC) with a relative foam density of 0.97 is four times that of its solid counterpart [9]. Furthermore, since the gas fills the interstitial sites between polymer molecules, it effectively reduces the viscosity [10–12] and the glass transition temperature of the polymer melt [6, 12–14]. This enables the material to be processed at much lower pressure and temperature levels [6]. The lower pressures experienced with microcellular injection molding also correlates to a reduction in residual stresses in the part, increasing the dimensional stability. Along with this decrease in residual stresses, the internal pressure arising from

Correspondence to: Lih-Sheng Turng; e-mail: turng@engr.wisc.edu
Contract grant sponsor: National Science Foundation; contract grant numbers: DMI 0140396; DMI 0323059; contract grant sponsor: UW-Madison Graduate School I&EDR Award.
DOI 10.1002/pen.20410
Published online in Wiley InterScience (www.interscience.wiley.com).
© 2005 Society of Plastics Engineers

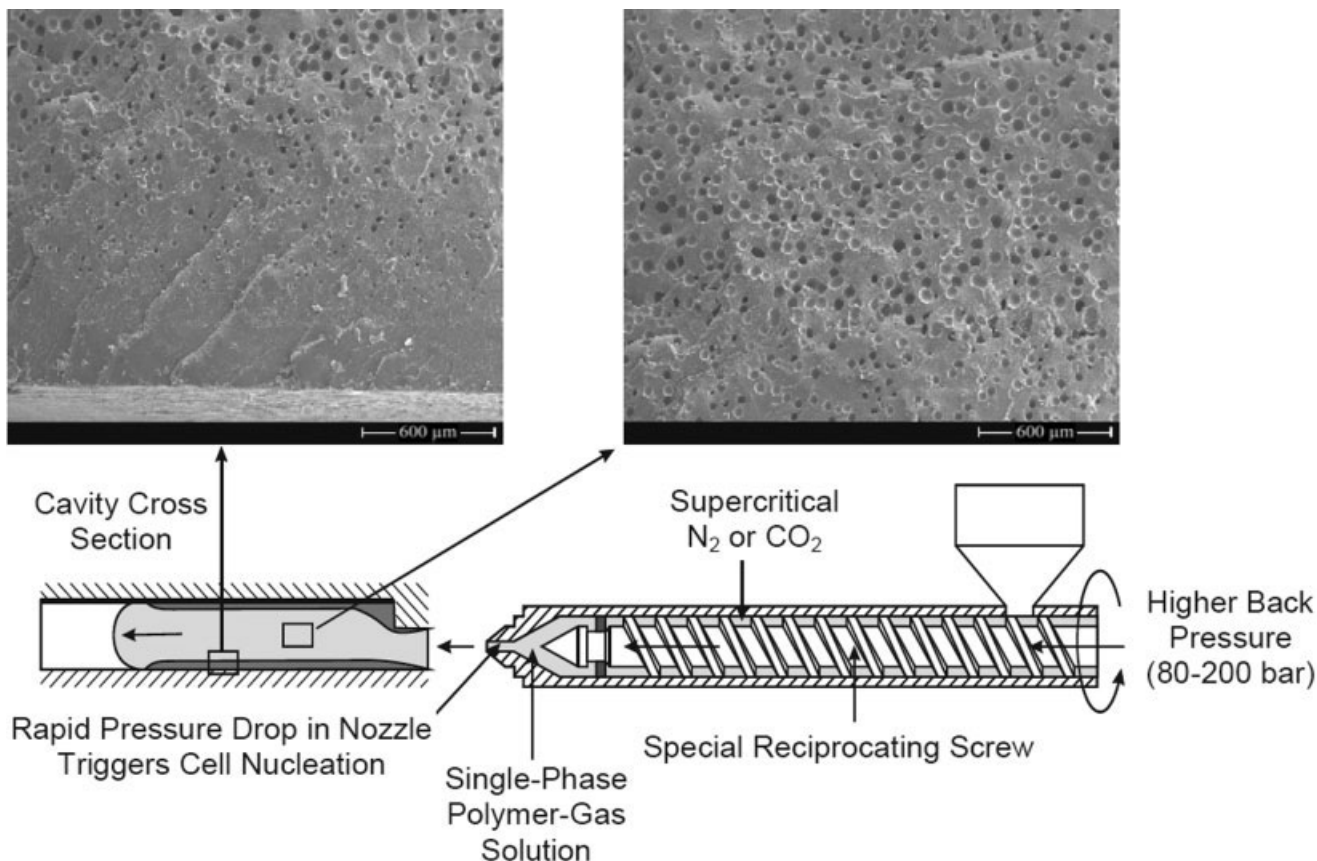


FIG. 1. Schematic of injection molding of microcellular plastics with characteristic microstructures.

foaming eliminates sink marks and further improves the dimensional stability of the molded parts. This internal pressure is not only homogenous throughout the part, it continues to pack the part against the mold walls until the polymer has solidified. As a result, the packing stage is eliminated, or greatly reduced (<0.5 s) in order to ramp the injection pressure from its injection phase to its recovery phase. This differs from conventional injection molding, where a large pressure gradient exists from the gate to the end of fill, and the packing of the cavity only exists until the gate freezes off. This packing time is usually determined by a gate freeze study in conventional injection molding. Another major benefit of microcellular injection molding is the cycle time reduction due to lower processing temperatures, the endothermic reaction of cell nucleation and growth, and the rapid solidification of polymer melt resulting from the recovery of the material's transition temperature as gas diffuses out from the solution [15]. Additional descriptions of this unique process can be found in Refs. 15 and 16 and references therein.

Despite these aforementioned benefits, microcellular injection molding is by no means a panacea for all molding problems or superior to its conventional counterpart in all aspects. As discussed in Ref. 15, the major challenges in processing MCPs lie in continuous and efficient generation of single-phased polymer-gas solution with proper gas content as well as control of the state of thermodynamic insta-

bility (via temperature and pressure variation) to create fine and uniform microcells throughout the part. At present, the process requires changes in the machinery components and the purchase of patent licenses [17]. Owing to the presence of microcells, it may have limited applications with parts that require optical clarity. In addition, the frequently occurring swirling patterns on part surfaces could potentially affect the cosmetic appearance. Nevertheless, it should be pointed out that the surface quality can be improved by hindering cell growth on injection by pressurizing the cavity (counterpressure), employing a hot mold surface during filling, or using coinjection molding to mold a smooth, solid (unfoamed) skin over the microcellular core [3]. Further, as with other emerging processes, the processing know-how for microcellular injection molding has yet to be fully developed by proper DOE applications to enable the molding industry to materialize the maximal process benefits. Finally, the cellular microstructure may adversely change the mechanical properties of the molded part. This is particularly true for tensile and weld-line strengths of injection-molded microcellular parts as less material is present due to foaming, low processing temperatures, and the absence of high-pressure packing of the mold.

The factors affecting dimensional stability in conventional injection molding have been widely studied and a wealth of information is available (see, e.g., Refs. 18, 19). However, while it is widely agreed upon that microcellular

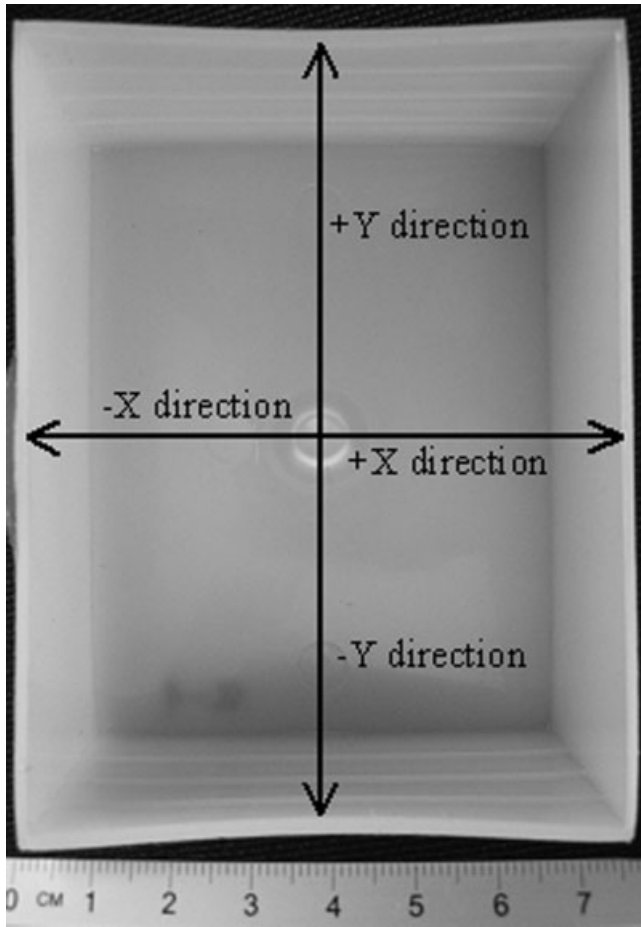


FIG. 2. Photo of a typical box-shaped part molded with conventional injection molding. Note the warp of the walls due to the box geometry, nonuniform wall thickness, and the semicrystalline PP resin. Thickness variation in the $-Y$ wall can be seen in the photo.

injection molding improves many aspects of part quality, no previous quantitative studies have reported on what process parameters affect the dimensional stability and at what magnitude. Furthermore, when examining dimensional stability and shrinkage and warpage (S&W), systematic, rigorous statistical studies have to be performed to compare conventional and microcellular injection molding, which motivated this study. It is widely known that pack/hold pressure and pack/hold time are two process parameters that

TABLE 1. Independent process parameters and their high and low settings for conventional injection molding.

Parameter settings for conventional injection molding experiment		
Parameter	Low (-1)	High (+1)
A—Hold time (sec)	3	6
B—Cooling time (sec)	20	35
C—Injection speed (mm/sec)	40	100
D—Hold pressure (bar)	400	600
E—Max barrel temp ($^{\circ}\text{C}$)	205	230
F—Chiller temp ($^{\circ}\text{C}$)	20	40

TABLE 2. Independent process parameters and their high and low settings for microcellular injection molding.

Parameter settings for microcellular injection molding experiment		
Parameter	Low (-1)	High (+1)
A—SCF dosage time (sec)	4	7
B—Shot volume (cm^3)	51	53
C—Max barrel temp ($^{\circ}\text{C}$)	205	230
D—Injection speed (mm/sec)	40	120
E—Chiller temp ($^{\circ}\text{C}$)	20	40
F—Cooling time (sec)	32	44

have a large effect on S&W in conventional injection molding. However, these two parameters are not present with microcellular injection molding. With basic microcellular injection molding knowledge it can be assumed that the amount of foaming that occurs in the cavity due to the SCF content has a large effect on the S&W, yet other parameters such as melt temperature, injection speed, and mold temperature may also play a role in the formation and growth of these microcells. This research studies the effect of various process parameters on the S&W of a specially built box part with polypropylene (PP). A 2^{6-1} fractional factorial DOE was performed for each process and the molded parts were tested and analyzed, as described in the following sections.

MATERIALS AND METHODS

To study the worst-case scenario and to be fair to both processes, a PP resin, ExxonMobil (Houston, TX) PP7032E2, injection molding grade, was selected for this study. It was anticipated that the S&W of the semicrystal-

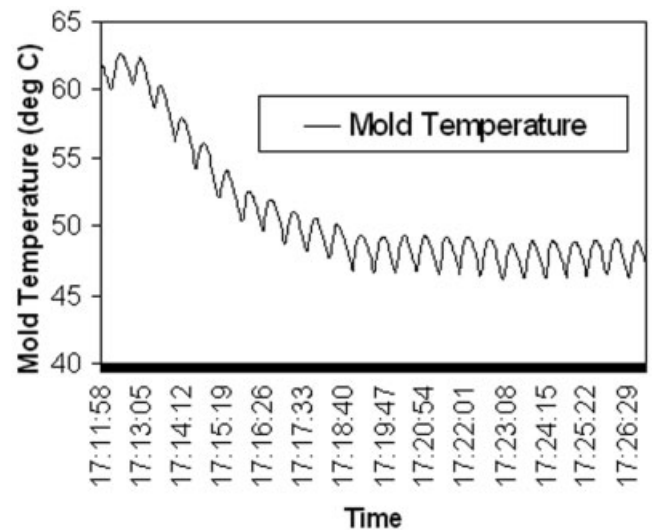


FIG. 3. Graph of mold temperature as a function of time. The cyclic nature of the graph is due to the injection and ensuing cooling of the polymer. Note the mold temperature decreases from a steady-state condition at the first set of parameters and then achieves steady state at the second set of parameters.

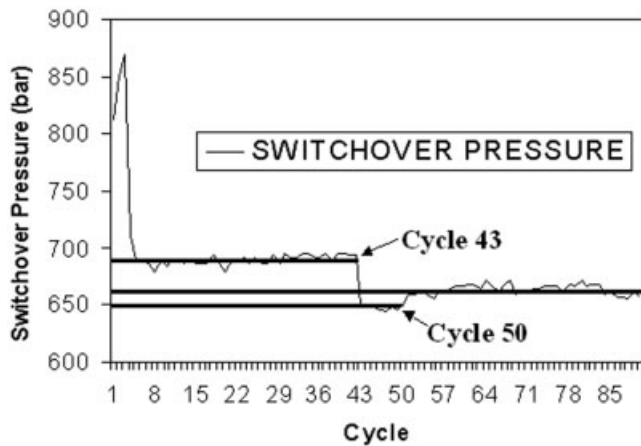


FIG. 4. Graph of the switchover pressure, which can be used to indirectly measure the viscosity of the material. Process changes were made at cycles 43 and 50, resulting in switchover pressure changes of ~ 30 and 20 bar, respectively.

line PP resin would be more significant than amorphous materials for conventionally injection molded parts. On the other hand, due to its semicrystalline structure and the fact

that PP has a weak melt strength, it is difficult to foam when compared to other plastics [20]. For the microcellular injection molding experiment, the PP was hand-blended with talc to obtain a mixture of 1 wt% talc. The talc acts as a nucleating agent and results in a smaller cell size as well as a greater cell density.

Experimental Setup and Procedure

In this study, two sets of six process parameters that can be independently controlled and adjusted for both microcellular and conventional injection molding were selected to study their effects on the S&W of a PP box part in four directions (cf. Fig. 2). The walls perpendicular to the x-direction were 1.3 mm thick and the walls perpendicular to the y-direction had four stepwise changes in thickness of 3.5 mm, 3 mm, 2.5 mm, and 2 mm. The overall outside dimensions of the part were $7.4 \times 9.8 \times 4.5$ cm.

The process parameters and the two levels of setting for conventional and microcellular injection molding are shown in Tables 1 and 2, respectively. Note that the "Maximum Barrel Temperature" is often referred to as melt temperature

TABLE 3. Standard matrix for 2^{6-1} DOE used for conventional injection molding.

Standard order	Hold time (sec) (A)	Cooling time (sec) (B)	Injection speed (mm/sec) (C)	Hold pressure (bar) (D)	Maximum barrel temperature ($^{\circ}$ C) (E)	Chiller temperature ($^{\circ}$ C) (F)	Trial number
1	3	20	40	400	205	20	29
2	6	20	40	400	205	40	7
3	3	35	40	400	205	40	18
4	6	35	40	400	205	20	5
5	3	20	100	400	205	40	30
6	6	20	100	400	205	20	9
7	3	35	100	400	205	20	27
8	6	35	100	400	205	40	19
9	3	20	40	600	205	40	21
10	6	20	40	600	205	20	12
11	3	35	40	600	205	20	11
12	6	35	40	600	205	40	20
13	3	20	100	600	205	20	13
14	6	20	100	600	205	40	28
15	3	35	100	600	205	40	6
16	6	35	100	600	205	20	10
17	3	20	40	400	230	40	17
18	6	20	40	400	230	20	14
19	3	35	40	400	230	20	4
20	6	35	40	400	230	40	16
21	3	20	100	400	230	20	1
22	6	20	100	400	230	40	25
23	3	35	100	400	230	40	26
24	6	35	100	400	230	20	3
25	3	20	40	600	230	20	8
26	6	20	40	600	230	40	23
27	3	35	40	600	230	40	22
28	6	35	40	600	230	20	24
29	3	20	100	600	230	40	2
30	6	20	100	600	230	20	15
31	3	35	100	600	230	20	32
32	6	35	100	600	230	40	31

The trial number on the right was assigned via a random number generator.

TABLE 4. Standard matrix for 2^{6-1} DOE used for microcellular injection molding.

Standard order	SCF dosage time (sec) (A)	Shot volume (cm ³) (B)	Maximum barrel temperature (°C) (C)	Injection speed (mm/sec) (D)	Chiller temperature (°C) (E)	Cooling time (sec) (F)	Trial number
1	4	51	205	40	20	32	13
2	7	51	205	40	20	44	14
3	4	53	205	40	20	44	6
4	7	53	205	40	20	32	7
5	4	51	230	40	20	44	21
6	7	51	230	40	20	32	16
7	4	53	230	40	20	32	5
8	7	53	230	40	20	44	18
9	4	51	205	120	20	44	28
10	7	51	205	120	20	32	20
11	4	53	205	120	20	32	11
12	7	53	205	120	20	44	1
13	4	51	230	120	20	32	26
14	7	51	230	120	20	44	17
15	4	53	230	120	20	44	2
16	7	53	230	120	20	32	27
17	4	51	205	40	40	44	29
18	7	51	205	40	40	32	31
19	4	53	205	40	40	32	9
20	7	53	205	40	40	44	15
21	4	51	230	40	40	32	19
22	7	51	230	40	40	44	32
23	4	53	230	40	40	44	3
24	7	53	230	40	40	32	25
25	4	51	205	120	40	32	30
26	7	51	205	120	40	44	10
27	4	53	205	120	40	44	22
28	7	53	205	120	40	32	8
29	4	51	230	120	40	44	4
30	7	51	230	120	40	32	24
31	4	53	230	120	40	32	12
32	7	53	230	120	40	44	23

The trial number on the right was assigned via a random number generator.

and the “Chiller Temperature” is often associated with mold wall temperature. In this article, chiller temperature was used as an independent process parameter and mold wall temperature was used as a response used to determine steady-state conditions for the process.

Due to the excessive time required to perform and analyze a full, 64-trial (2^6) DOE for each injection molding process, a 2^{6-1} fractional factorial design was employed for conventional and microcellular injection molding. This resolution VI (six) fractional factorial design means all main effects and two-factor interactions of the six process parameters are clear of each other, allowing them to be accurately estimated. These effects are only confounded with three-factor interactions and higher, and these can generally be assumed to be insignificant. Upper and lower settings of all process parameters were determined experimentally to create as large a process window as possible without creating defective parts, such as a short shot or post-blow (a surface blister defect in microcellular injection molding). In addition to experimentally determining the proper process parameters, a steady-state condition needed to be determined before collecting parts for each molding trial. In this study,

the mold temperature was monitored to help determine when the process had reached steady state. It was also determined through preliminary experimentation and a 2^3 factorial design that the mold temperature was most strongly affected by chiller temperature, followed by cooling time and maximum barrel temperature. Most important, graphs indicating the steady state mold temperature were generated and used during the experiment. Figure 3 shows

TABLE 5. Intraclass correlation coefficients (ICC) and discrimination ratios (D_R) for the four measurement directions.

GAGE Repeatability and Reproducibility (GAGE R&R)		
Measurement direction	ICC	D_R
-X	0.940	5.68
+X	0.979	9.69
-Y	0.982	10.40
+Y	0.983	10.76

The lower D_R for the -X direction can be attributed to excess flash on that side, making determining the actual edge of the part less accurate.

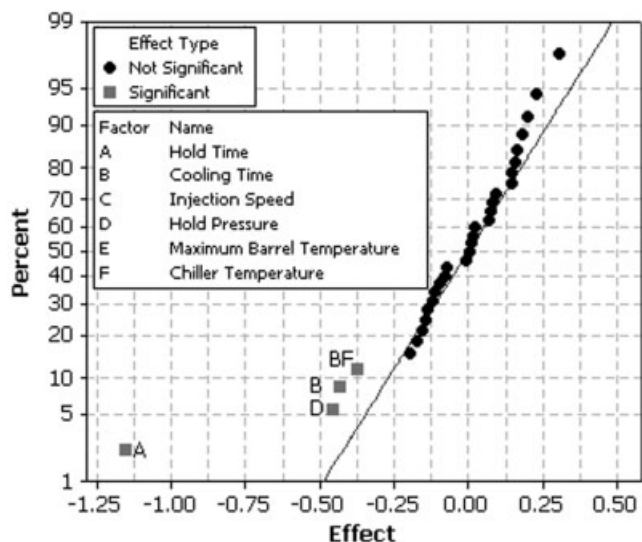


FIG. 5. Graphical method, called Normal Probability Plot, used for determining significant main and interaction effects. Effects for -X warp with conventional injection molding is shown in this plot.

the cyclic change, as well as the overall mold temperature decrease, when the chiller temperature setting is changed from 40°C to 20°C, with all other parameters remaining constant.

In addition to monitoring the mold temperature, the switchover pressure was also used to determine the steady-state condition. The switchover pressure is the injection pressure at the point where the injection phase changes from velocity control to pressure control, or in microcellular injection molding, from velocity control to screw recovery (due to the absence of the packing stage in the microcellular injection molding process). This pressure is an indication of the viscosity of the material and considerable shifts in switchover pressure were observed between molding trials when performing the microcellular injection molding experiment. An example of monitoring switchover pressure can be seen in Fig. 4. Note the abrupt shift in switchover pressure at cycles 43 and 50, which directly correspond to process changes. Using mold temperature and switchover pressure, steady-state conditions corresponding to all of the molding trials were determined during preliminary experiments. During the running of both DOEs, the process conditions observed between molding trials were checked against the predetermined steady state conditions. Once the current and predetermined steady state conditions matched, 10 parts were collected for that molding trial. In order to improve the accuracy of the experiments, this method was used in place of arbitrarily selecting a number of parts to discard between each molding trial. It was observed that the actual mold temperatures obtained during the DOE were within $\pm 1^\circ\text{C}$ of the steady state mold temperatures determined during preliminary experiments.

Two DOE matrices were constructed for conventional injection molding and microcellular injection molding, as shown in Tables 3 and 4, respectively. According to Ref. 21,

randomization is the cornerstone underlying the use of statistical methods in experimental design, and it assists in “averaging out” the effects of extraneous factors that may be present. Noting this, a random number generator was used to determine the order in which the trials were run. Separate sheets detailing each run of the experiment were also developed and used to eliminate human error when changing process parameters during the experiment. This was also used to record any abnormal phenomena that occurred throughout the experiment, which could then be interpreted and lead to further insight into the cause of an error. An example of determining the cause of error during this experiment and nullifying its effects is discussed in the measurement and analysis section.

During both DOEs, a total of 10 parts were collected and individually labeled after achieving steady-state conditions for each of the 32 trials. These parts were placed in marked boxes for several weeks before measuring the S&W. The measurement procedure for acquiring the S&W on this part was extremely involved, and in order to provide accurate data without fatigue skewing the results, part numbers 5–9 were measured and the average obtained for each trial.

While the shrinkage and warpage were grouped into an S&W term in this research, the shrinkage was also investigated as its own entity. The shrinkage was measured using a digital caliper on the closed side of the box part, where there was no measurable deformation of the part. A comparison of the conventionally injection molded parts and the microcellular injection-molded parts did not show a statistically significant difference in the shrinkage of the box part. Therefore, the more accurate measurement of the box part using an optical coordinate measuring machine (OCMM) is used to describe the S&W as one entity.

The S&W of the box part was measured by an OCMM with accuracy down to 2.5 microns; the use of any physical

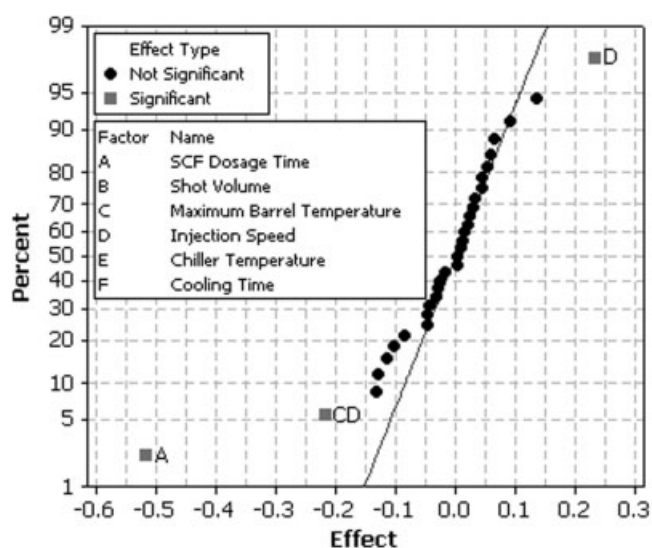


FIG. 6. Graphical method, called Normal Probability Plot, used for determining significant main and interaction effects. Effects for -X warp with microcellular injection molding is shown in this plot.

TABLE 6. Regression models derived for conventional injection molding experiment.

Conventional injection molding experiment	
Response	Regression model
-X	$\hat{Y} = 0.8093 - 0.5763A - 0.2291D - 0.2154B - 0.1877BF - 0.0853F$
+X	$\hat{Y} = -0.1827 - 0.8455A - 0.3165D - 0.2341B - 0.2236BF - 0.0308F$
-Y	$\hat{Y} = 1.3784 - 0.2096D - 0.1924A - 0.1400AD$
+Y	$\hat{Y} = 1.4204 - 0.2887D - 0.1962A - 0.1123AD$

means of measurement that involves contacting the parts would have distorted the walls and adversely affected the accuracy of the S&W measurements. A fixture was fabricated and mounted to the machine base in order to reduce error involved in the measurement process. A center position was determined for each part by determining the x,y-plane of the fixture and selecting several locations around a witness line from a pressure transducer location (which was near the center of the part). A measurement was then taken in each of the four directions (cf. Fig. 2). Each of these four measurements was then subtracted from a predetermined CAD dimension, quantitatively defining the amount of S&W in each direction.

Measurement and Analysis

The success of using DOE to improve product quality and productivity depend highly on the accuracy and precision of the measurements. If the data collected are not accurate and precise, they do not represent the true characteristics of the parts being measured even though manufacturers are using the quality tools correctly [22]. Therefore, it is very important to have valid measurement studies to ensure that the data and measurements collected are accurate and precise, so that the effectiveness of DOE is fully utilized. For this research, GAGE R&R (Gage repeatability and reproducibility) studies were performed for each of the four measurements. Two ratios, called the intraclass correlation coefficient (ICC) and the discrimination ratio (D_R) can be used to determine the capability of the measurement process [23]. A measurement process with a D_R greater than four denotes that the measurement process is capable to detect significant product variation [22, 23]. The ICC can also be used to determine a valid measurement process, but it does not contain the appraiser variation (A.V.). Using a system with two trials and two operators, the D_R was found

to be well above four for each of the four directions, with the actual values given in Table 5. Note that the lower value of 5.68 in the -X direction can be attributed to an abundance of flash when compared to the other three directions, making determining the exact edge more challenging. When not taking the part variation into account, it was determined that the actual measurement variation was ~0.07 mm in the X-directions and 0.05 mm in the Y-directions. For a detailed description of how to accurately perform a GAGE R&R study, refer to Refs. 22 and 23.

DOE analysis software (Minitab) was used to analyze the data collected from both experiments. Because the unrepliated experiments were employed, a graphical method called Normal Probability Plot was used to determine significant main and interaction effects. The effects that are negligible are normally distributed, with mean zero and variance σ^2 and will tend to fall along a straight line on this plot, whereas significant effects will have nonzero means and will not lie along the straight line [21]. This analysis was performed for all four measurements (+X, -X, +Y, -Y) for each process. Figures 5 and 6 are normal probability plots depicting significant main and interaction effects in the -X direction for conventional and microcellular injection molding, respectively.

Using the significant main and interaction effects, multiple linear regression models were derived for each of the four directions for each process. Tables 6 and 7 display the regression models derived for the conventional and microcellular injection molding experiments. A regression model is a mathematical model used to predict the response. For example, if main effect A, main effect B, and interaction effect AC are all deemed significant, the regression model will look like:

$$\hat{Y} = b_0 + b_A X_A + b_B X_B + b_{AC} X_A X_C \tag{1}$$

where: \hat{Y} = predicted response; b_0 = average response for

TABLE 7. Regression models derived for microcellular injection molding experiment.

Microcellular injection molding experiment	
Response	Regression model
-X	$\hat{Y} = 0.4131 - 0.2583A + 0.1164D - 0.1089CD - .0419C$
+X	$\hat{Y} = 0.4489 - 0.2790A + 0.0961D + 0.0749B - 0.0661CD - 0.0582C$
-Y	$\hat{Y} = 0.2648 - 0.1227A - 0.0647D - 0.0372C + 0.0302CD - 0.0207AD - 0.0139E$
+Y	$\hat{Y} = 0.1256 - 0.0652A + 0.0276AC - 0.0212B - 0.0197DE - 0.0102C + 0.0043E + 0.0025D$

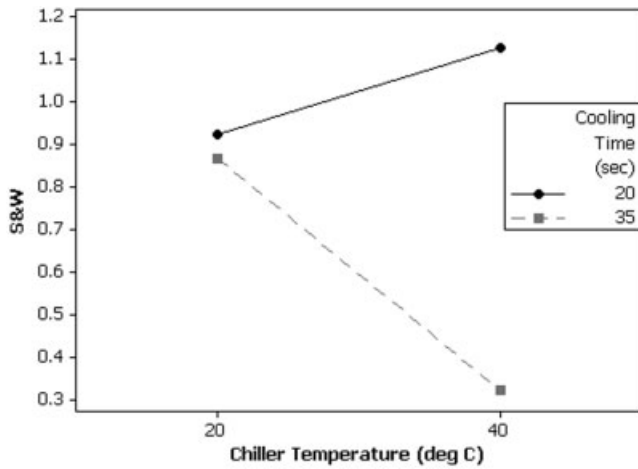


FIG. 7. Interaction plot indicating that an increase in chiller temperature and an increase in cooling time will yield the S&W closest to zero in the -X direction with conventional injection molding.

all trials; $b_A = \frac{E_A}{2}$ = effect of independent variable A divided by 2; $b_{AC} = \frac{E_{AC}}{2}$ = effect resulting from interaction between variables A and C divided by 2; X_A = the level of independent variable A, either -1 (low setting) or +1 (high setting). Actual regression models can be seen in Tables 6 and 7. The predicted response, \hat{Y} , is then subtracted from the observed response, Y , to give the residual error, ϵ . This was done for all 32 trials of the experiment for both processes. The residuals should be centered about a mean of zero and should be normally distributed. A series of tests/checks were performed on the residuals to ensure that they behaved as they should in order to prove that the regression models were adequate. During these tests it was found that high residual error existed for four trials of the conventional injection molding experiment. Reviewing the comments

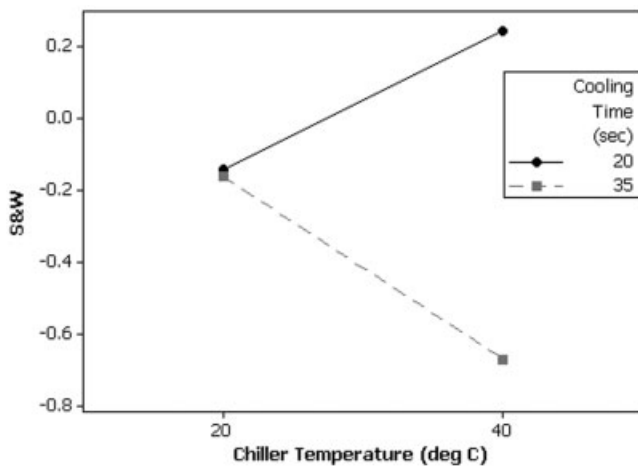


FIG. 8. Interaction plot indicating that a decrease in chiller temperature and either the high or low setting for cooling time will yield the S&W closest to zero in the +X direction with conventional injection molding.

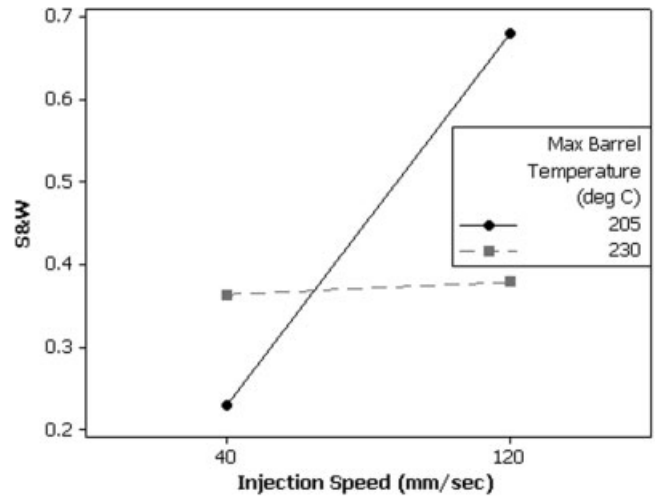


FIG. 9. Interaction plot indicating that a decrease in injection speed and a decrease in maximum barrel temperature will yield the S&W closest to zero in the -X direction with microcellular injection molding.

and data from the experiment did not reveal anything out of the ordinary. However, during the measurement process a note was attached to the four trials stating that a mistake was made measuring the last two parts of each five-piece trial. Examining the data showed a drastic difference between part numbers 1-3 and 4-5, and therefore, for the conventional molding experiment, only three parts were used for the analysis. During the retesting of the residual error with three parts the error was seen to be greatly reduced or nonexistent (over the course of all 32 trials), therefore proving the adequacy and usefulness of our regression model. At this time the authors would like to point out the problem-solving capability of DOE. By analyzing the data the inconsistency in measuring the parts was discovered. From proper recording of the experiment and measurement of the parts the cause for the inconsistency was found and

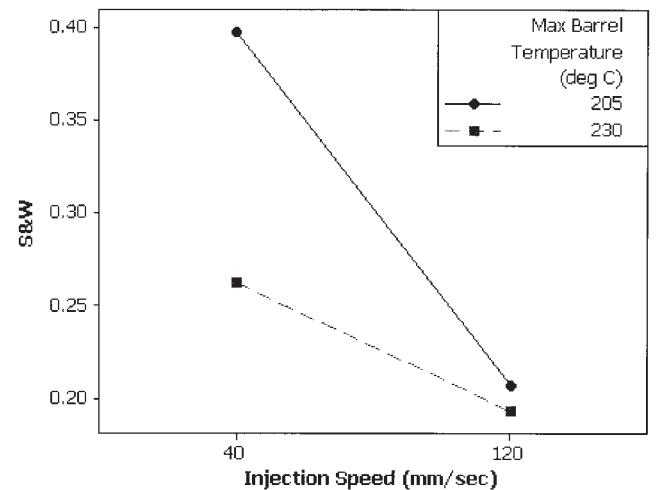


FIG. 10. Interaction plot indicating that an increase in injection speed and an increase in maximum barrel temperature will yield the S&W closest to zero in the -Y direction with microcellular injection molding.

TABLE 8. The three best combinations of parameter settings for obtaining the minimum S&W and the predicted average S&W (conventional injection molding).

Parameter settings and resulting S&W (conventional injection molding)						
Hold time (sec)	Cooling time (sec)	Inj. speed (mm/sec)	Hold pressure (bar)	Max. barrel temp. (°C)	Chiller temp. (°C)	S&W _{avg} (mm)
6	20	Not significant	600	Not significant	40	0.727
6	35	Not significant	600	Not significant	20	0.760
6	20	Not significant	600	Not significant	20	0.768

corrected, resulting in greatly improved results and conclusions.

It was found that the pack/hold time and the pack/hold pressure had the most significant effect on the S&W, respectively, in all directions for the conventional injection molding process. In addition, it was determined that an interaction effect existed between the chiller temperature and the cooling time in the -X and +X directions. The interaction effects in the -X and +X directions can be seen in Figs. 7 and 8, respectively. The regression models derived previously were then used to determine the optimal parameter settings for producing the box with the S&W closest to zero. This consisted of using all four regression models with the same parameter settings, then averaging the absolute value of the warp in all four directions to determine the average S&W of the walls. It can be seen from Figs. 7 and 8 that the optimal parameters for achieving S&W closest to zero are different for the -X and +X directions. In the -X direction the maximum chiller temperature and maximum cooling time resulted in the minimum S&W. In the +X direction the minimum chiller temperature will result in the minimum S&W, with the cooling time being insignificant at the minimum chiller temperature. Therefore, compromises were made in order to achieve the least overall S&W for the box part.

In the microcellular injection molding experiment, the wt% SCF content (in terms of SCF dosage time) had the most significant effect on the S&W, as shown in Fig. 6. The SCF dosage times used for this experiment correlated to

~0.33 and 0.59 wt% SCF content. Additionally, an interaction effect existed between the injection speed and the maximum barrel temperature (melt temperature) (Fig. 9). Examining the data indicates that decreasing the injection speed at the low barrel temperature has a significant impact on decreasing S&W in the X-direction, while an increase in injection speed at the high barrel temperature setting reduces S&W in the Y-direction. This can be seen more clearly in Figs. 9 and 10, which show this interaction effect in the -X and -Y directions, respectively. Such an opposite effect is believed to be due to the difference in wall thickness, the degree of race-tracking due to changes in injection speed and barrel temperature, and the parts response to S&W in both X and Y directions. In general, a higher injection speed leads to a higher pressure drop rate, resulting in higher cell density. On the other hand, lower melt temperature increases the melt strength, hampers cell coalescence, and reduces the degree of race-tracking in the box part. Again, a compromise must be made when determining optimal variable settings for this experiment.

RESULTS AND DISCUSSION

While the process parameters and their settings varied slightly between experiments, the process window was as large as possible for each experiment, hindered only by the production of defective parts. Therefore, not only was it possible to compare the S&W values at optimal parameter

TABLE 9. The three best combinations of parameter settings for obtaining the minimum S&W and the predicted average S&W (microcellular injection molding).

Parameter settings and resulting S&W (microcellular injection molding)						
SCF dosage time (sec)	Shot volume (cm ³)	Max. barrel temp. (°C)	Inj. speed (mm/sec)	Chiller temp. (°C)	Cooling time (sec)	S&W _{avg} (mm)
7	51	230	120	40	Not significant	0.077
7	51	230	120	20	Not significant	0.092
7	51	205	40	20	Not significant	0.096

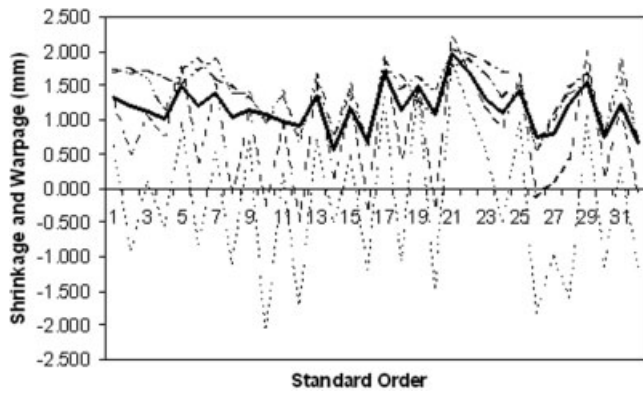


FIG. 11. S&W in each direction over the course of the 32 standard trials as well as the average S&W (bold line) for the conventional injection molding process determined from the absolute value of all four directions.

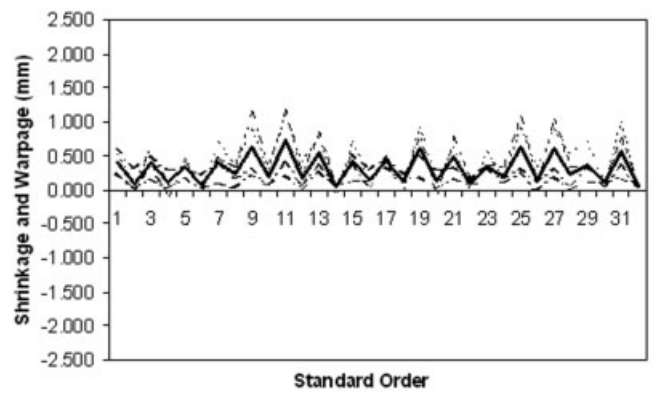


FIG. 12. S&W in each direction over the course of the 32 standard trials as well as the average S&W (bold line) for the microcellular injection molding process determined from the absolute value of all four directions.

settings, but also to show the variation in S&W over the course of the DOE, or all 32 trials.

To begin with the overall S&W, Table 8 lists several

combinations of parameters and their calculated values (using the multiple linear regression models) found for conventional injection molding. It can be seen that at the

TABLE 10. Standard deviation examined for all 32 molding trials.

Conventional injection molding					Microcellular injection molding				
Standard order	-X	+X	-Y	+Y	Standard order	-X	+X	-Y	+Y
1	0.076	0.068	0.020	0.036	1	0.106	0.035	0.051	0.037
2	0.144	0.039	0.096	0.028	2	0.089	0.092	0.033	0.029
3	0.071	0.029	0.130	0.067	3	0.086	0.052	0.009	0.022
4	0.135	0.041	0.176	0.104	4	0.022	0.043	0.020	0.019
5	0.111	0.137	0.046	0.159	5	0.044	0.127	0.031	0.017
6	0.053	0.042	0.060	0.049	6	0.066	0.044	0.019	0.014
7	0.086	0.018	0.035	0.032	7	0.092	0.027	0.016	0.013
8	0.041	0.080	0.081	0.046	8	0.028	0.088	0.009	0.031
9	0.099	0.110	0.057	0.018	9	0.120	0.202	0.055	0.044
10	0.038	0.166	0.032	0.029	10	0.134	0.073	0.042	0.038
11	0.115	0.062	0.039	0.047	11	0.117	0.060	0.027	0.030
12	0.199	0.050	0.044	0.017	12	0.087	0.077	0.032	0.039
13	0.134	0.027	0.016	0.126	13	0.152	0.193	0.050	0.031
14	0.074	0.044	0.041	0.036	14	0.100	0.026	0.044	0.041
15	0.083	0.071	0.068	0.121	15	0.039	0.047	0.023	0.011
16	0.078	0.075	0.039	0.015	16	0.172	0.066	0.023	0.017
17	0.113	0.092	0.056	0.046	17	0.048	0.098	0.060	0.058
18	0.127	0.121	0.093	0.107	18	0.084	0.030	0.032	0.020
19	0.301	0.089	0.053	0.077	19	0.081	0.065	0.022	0.025
20	0.136	0.106	0.137	0.006	20	0.071	0.074	0.042	0.025
21	0.023	0.171	0.158	0.182	21	0.161	0.123	0.028	0.017
22	0.046	0.198	0.043	0.045	22	0.043	0.025	0.016	0.004
23	0.058	0.080	0.037	0.018	23	0.029	0.016	0.017	0.031
24	0.281	0.403	0.331	0.313	24	0.069	0.068	0.047	0.012
25	0.004	0.024	0.013	0.022	25	0.107	0.108	0.027	0.020
26	0.026	0.128	0.039	0.028	26	0.051	0.027	0.007	0.021
27	0.100	0.030	0.050	0.048	27	0.182	0.264	0.049	0.032
28	0.052	0.147	0.032	0.018	28	0.076	0.075	0.013	0.020
29	0.060	0.201	0.047	0.075	29	0.095	0.042	0.022	0.019
30	0.124	0.077	0.088	0.005	30	0.063	0.038	0.016	0.031
31	0.044	0.012	0.029	0.024	31	0.155	0.091	0.016	0.016
32	0.115	0.054	0.040	0.025	32	0.028	0.047	0.035	0.037
Avg. SD (mm)	0.098	0.093	0.070	0.061	Avg. SD (mm)	0.088	0.076	0.029	0.026

The data suggests microcellular injection molding provides greater dimensional stability when compared to conventional injection molding (less sensitive to uncontrolled variables).

optimal parameter settings for minimizing the S&W, the predicted average warp for each of the walls was 0.727 mm. Table 9 lists several combinations of parameters and their calculated values (using the multiple linear regression models) found for microcellular injection molding. It can be seen that at the optimal parameter settings for minimizing the S&W the predicted average warp for each of the walls was 0.077 mm. Therefore, using microcellular injection molding at the optimal parameter settings, the average S&W for each wall decreased by 0.650 mm, or 89%, when compared to conventional injection molding at the optimal parameter settings. Verification trials were run after the analysis was performed in order to verify the original experiment.

The actual S&W measurements for conventional and microcellular injection molding can be seen in Figs. 11 and 12, respectively. The standard deviation over the course of all 32 trials was also examined for both processes and can be seen in Table 10. Table 10 displays the standard deviation of the five parts measured and the average of that standard deviation over all 32 trials. It is seen that the standard deviation for all four measurements decreases with microcellular injection molding. This suggests that, under steady process conditions, the microcellular injection molding process offers better dimensional stability and less part-to-part variation than the conventional injection molding process. Examination of Figs. 11 and 12 indicates that, within the processing range studied, the S&W of the box part is less sensitive to changes in parameter settings and much closer to zero with microcellular injection molding than with conventional injection molding.

CONCLUSIONS

Proper planning, execution, and analysis of design of experiments are essential for determining statistically significant main and two-factor interaction effects. By adhering to these principles, this study quantitatively showed a decrease in S&W can be achieved using microcellular injection molding when compared to conventional injection molding. The results suggest that the supercritical fluid content (%SCF, in terms of SCF dosage time) and injection speed affect the S&W of microcellular injection-molded parts most significantly. When examining conventional injection molding, the results suggest that the hold pressure and hold time have the most significant effect on the S&W. The variability from part to part at constant variable settings also appears to be less with microcellular injection molding when compared to conventional injection molding. This study also quantitatively showed that, within the processing range studied under all processing conditions, a reduction in the S&W could be achieved with the microcellular injection molding process.

ACKNOWLEDGMENTS

We thank EVCO Plastics for the use of their optical coordinate measuring machine (OCMM) for taking the S&W measurements, as well as ExxonMobil and Moog Japan and Cornell Injection Molding Program (CIMP) for donating the polypropylene and box mold, respectively, used for the experiments.

REFERENCES

1. A. Chandra, S. Gong, M. Yuan, L.S. Turng, P. Gramman, and H. Cordes, *Polym. Eng. Sci.*, **45**, 52 (2005).
2. A. Chandra, S. Gong, L.S. Turng, and P. Gramman, *J. Cell. Plastics*, **40**, 371 (2004).
3. H. Kharbas and L.S. Turng, *Int. Polym. Proc.*, **19**, 77 (2004).
4. M. Yuan, L.S. Turng, D. Caulfield, C. Hunt, and R. Spindler, *Polym. Eng. Sci.*, **44**, 673 (2004).
5. H. Kharbas, P. Nelson, M. Yuan, S. Gong, L.S. Turng, and R. Spindler, *Polym. Compos.*, **24**, 655 (2003).
6. N.P. Suh, "Microcellular Plastics," in *Innovation in Polymer Processing-Molding*, J.F. Stevenson, ed., Hanser Publishers, Munich, 93 (1996).
7. C.B. Park, S. Doroudiani, and M.T. Kortschot, *Polym. Eng. Sci.*, **38**, 1205 (1998).
8. M. Shimbo, D.F. Baldwin, and N.P. Suh, *Polym. Eng. Sci.*, **35**, 1387 (1995).
9. K.A. Seeler and V. Kumar, *J. Reinf. Plastics Compos.*, **12**, 359 (1993).
10. C. Kwag, C.W. Manke, and E. Gulari, *J. Polym. Sci., Part B: Polym. Phys.*, **37**, 2771 (1999).
11. J.R. Royer, Y.J. Gay, J.M. Desimone, and S.A. Khan, *J. Polym. Sci., Part B: Polym. Phys.*, **38**, 3168 (2000).
12. C. Kwag, C.W. Manke, and E. Gulari, *Ind. Eng. Chem. Res.*, **40**, 3048 (2001).
13. Z. Zhang and Y.P. Handa, *J. Polym. Sci., Part B: Polym. Phys.*, **37**, 977 (1998).
14. Y.P. Handa, P. Kruus, and M. O'Neill, *J. Polym. Sci., Part B: Polym. Phys.*, **34**, 2635 (1996).
15. L.S. Turng, *J. Inject. Mold. Tech.*, **5**, 160 (2001).
16. J. Xu and D. Pierick, *J. Inject. Mold. Tech.*, **5**, 152 (2001).
17. Trexel, Inc., <http://www.trexel.com/>.
18. N. Santhanam, "Analysis of Residual Stresses and Post-Molding Deformation in Injection-Molded Components," Ph.D. Thesis, Cornell University, Ithaca, New York (1992).
19. N. Santhanam, H.H. Chiang, K. Himasekhar, P. Tuschak, and K.K. Wang, *Adv. Polym. Technol.*, **11**, 77 (1992).
20. C.B. Park and L.K. Cheung, *Polym. Eng. Sci.*, **37**, 1 (1997).
21. D.C. Montgomery, *Design and Analysis of Experiments*, John Wiley & Sons, New York (1997).
22. D.S. Ermer and R.Y. E-Hok, *Contributed Publications of the Measurement Quality Division*, American Society for Quality, Milwaukee, WI, 2 (1997).
23. D.J. Wheeler and R.W. Lyday, *Evaluating the Measurement Process*, SPC Press, Knoxville, TN (1989).